Indocyanine green-loaded perfluorocarbon nanoemulsions for bimodal ^{19}F-magnetic resonance/nearinfrared fluorescence imaging and subsequent phototherapy

Yuan-Guo Wang[1*], Hyunjin Kim[1*], Saehun Mun[2], Daehong Kim[1], Yongdoo Choi[1]

[1]Molecular Imaging and Therapy Branch, National Cancer Center, 323 Ilsan-ro, Goyang-si, Gyeonggi-do 410-769, Korea; [2]Center for Food and Bioconvergence, Department of Biosystems and Biomaterials Science and Engineering, Seoul National University, Seoul 151-742, Republic of Korea
*These authors contributed equally to this work.
Corresponding to: Yongdoo Choi, PhD. Molecular Imaging and Therapy Branch, National Cancer Center, Goyang-si, 410-769, Republic of Korea. Email: ydchoi@ncc.re.kr; Daehong Kim, PhD. Molecular Imaging and Therapy Branch, National Cancer Center, Goyang-si, 410-769, Republic of Korea. Email: dkim@ncc.re.kr.

Abstract: We have developed an indocyanine green-loaded perfluorocarbon (ICG/PFCE) nanoemulsion as a multifunctional theranostic nanomedicine which enables not only ^{19}F magnetic resonance (MR)/near-infrared fluorescence (NIRF) bimodal imaging but also subsequent photodynamic/photothermal dual therapy of cancer. The hydrodynamic size of ICG/PFCE nanoemulsions was 164.2 nm. The stability of indocyanine green (ICG) in aqueous solution was significantly improved when loaded on perfluorocarbon nanoemulsions. In addition, ICG/PFCE nanoemulsions showed good dispersion stability in aqueous media containing 10% fetal bovine serum, for at least 14 days.

^{19}F-MRI of ICG/PFCE nanoemulsions showed that the signal intensity increased with increasing nanoemulsion concentration with no signal observed from the surrounding background. Using NIRF imaging with perfluorocarbon nanoemulsion alone, without ICG, did not produce NIRF, while clear and bright fluorescent images were obtained with ICG/PFCE nanoemulsions at 10-μM ICG equivalent. The capacity of ICG-loaded nanoemulsions to generate heat following light irradiation by using an 810-nm laser was comparable to that of free ICG, while singlet oxygen generation of ICG-loaded nanoemulsions was significantly better than that of free ICG.

In vitro cytotoxicity tests and fluorescence microscopy confirmed biocompatibility of the nanoemulsion. Upon light irradiation, U87MG glioblastoma cells incubated with ICG/PFCE nanoemulsions underwent necrotic cell death. The therapeutic mechanism during light illumination appears to be mainly due to the photodynamic effect at lower ICG concentrations, whilst the photothermal effect became more obvious at increased ICG concentrations, enabling combined photodynamic/photothermal therapy of cancer cells.

Key Words: Indocyanine green; perfluorocarbon; ^{19}F-magnetic resonance imaging; near-infrared fluorescence imaging; photodynamic therapy; photothermal therapy

Introduction

Multifunctional nanomedicines have received widespread attention for their unique characteristics and potential as novel tools for simultaneous diagnosis and treatment of various diseases (1-3). In this study, we show the potential of indocyanine green-loaded perfluorocarbon nanoemulsions as a multifunctional theranostic nanomedicine that enables not only ^{19}F-magnetic resonance (MR)/near-infrared fluorescence (NIRF)
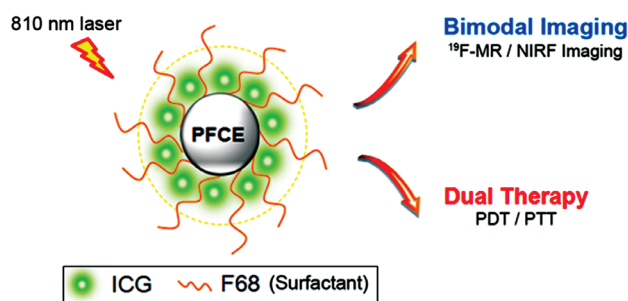
Figure 1 Schematic diagram of ICG/PFCE nanoemulsions as a multifunctional theranostic nanomedicine

bimodal imaging but also subsequent dual photodynamic therapy (PDT)/photothermal therapy (PTT) of cancer cells. The advantages of perfluorocarbon nanoemulsions for ^{19}F-MRI are as follows: (I) perfluorocarbons (PFCs) are well-known, biologically inert, organic molecules; (II) the sensitivity of fluorine for MRI is comparable to that of proton (i.e., 83% of ^{1}H); and (III) fluorine shows negligible ^{19}F background signal from tissues because of its very low background biological abundance (4-6). Therefore, PFC nanoemulsions can be used as a "tracer" for non-invasive ^{19}F-MRI with high spatial resolution and no depth limitation.

NIRF imaging, in spite of its limitation in imaging depth compared with the other modalities, has been considered a great tool for image-guided surgery because it has numerous advantages including real-time, non-invasive imaging, high sensitivity, easy-to-use, and detection without ionizing irradiation (7,8). Indocyanine green (ICG), a water-soluble tricarbocyanine dye, is the only clinically approved near-infrared (NIR) fluorophore along with methylene blue. ICG has been used in a variety of diagnostic applications including NIRF image-guided oncologic surgery, retinal angiography, lymph node detection in multiple types of cancers, and intraoperative identification of certain solid tumors (7,9,10). In addition, ICG has capability of producing singlet oxygen and heat upon NIR light irradiation, thus expanded its utility for PDT and PTT of cancers (10-12). However, concentration-dependent aggregation, irreversible degradation in aqueous solution, short blood half-life (2-4 min), and accelerated degradation in aqueous solution during light exposure decreases its therapeutic efficacy (13-15). In view of these limitations, many nanostructure-based ICG have been designed to improve its stability and tumor targeting efficiency (12,14,16). Recently, ICG-loaded multifunctional nanoparticles have been developed for

^{1}H-MR /NIRF bimodal imaging and PTT (17,18).

In this study, we have developed ICG-loaded perfluorocarbon nanoemulsion for ^{19}F-MR/NIRF bimodal imaging and combined PDT/PTT of cancer cells. In addition to beneficial properties as a ^{19}F-MRI agent and drug delivery carrier, PFCs also have high oxygen-dissolving capacities (~40-50 vol%), as compared with 2.5 vol% for water (19). Since consumption of oxygen molecules occurs during PDT, the supply of oxygen into target sites is highly important to generate as much reactive singlet oxygen as possible, thereby maximizing PDT efficacy. PFCs loaded with ICG may provide a good source of oxygen supply in addition to that from the blood stream. Among PFCs, perfluoro-15-crown-5-ether (PFCE) was selected for ^{19}F-MRI as PFCE consists of 20 equivalent fluorine nuclei having a single resonance at –92.5 ppm whereas other PFCs have multiple ^{19}F resonance peaks (6). A schematic illustration of the structure of the multifunctional ICG/PFCE nanoemulsions is shown in *Figure 1*.

Materials and methods

Materials

Indocyanine green (ICG, molar mass 774.96 g/mol), sodium dodecyl sulfate (SDS), and sodium hydroxide (NaOH) were purchased from Sigma-Aldrich Chemical Co. (St. Louis, USA). The surfactant Lutrol® F68 (poloxamer 188) was obtained from BASF (Ludwigshafen, Germany). Perfluoro-1, 5-crown-5-ether (PFCE, 580.08 g/mol) was purchased from Fluorochem (Derbyshire, UK). PD-10 desalting columns were purchased from Amersham Biosciences Corp. (Piscataway, NY). Singlet oxygen sensor green reagent (SOSG) and the Live/Dead Viability Calcein AM staining kit were obtained from Invitrogen Corp. The U87MG human malignant glioma cell line was obtained from the American Type Culture Collection (Rockville, USA) and maintained in Dulbecco's Modified Eagle Medium (DMEM) (GIBCO®, Invitrogen) supplemented with 10% (v/v) fetal bovine serum (FBS) and 1% antibiotic-antimycotic in a humidified 5% CO_2 incubator at 37 ℃.

Preparation of ICG/PFCE nanoemulsions and determination of ICG loading efficiency

To prepare ICG/PFCE nanoemulsions, PFCE (0.4 g), surfactant Lutrol® F68 (60 mg), and ICG (1 mg) were mixed and dispersed into phosphate-buffered saline

134

Wang et al. ICG/PFCE nanoemulsions for bimodal ^{19}F-MR/NIRF

(PBS; 6.7 mM, pH 7.4, NaCl 154 mM) solution. The mixture was emulsified by sonication for 20 min in ice cold water (VCX500, Sonics and Materials, Inc., CT, USA). Subsequently, free ICG was removed by passing the solution through a PD-10 column (PBS eluent, pH 7.4). To calculate the loading efficiency and concentration of ICG in the prepared emulsion, the emulsion dispersions were diluted with 0.1 M NaOH/0.1% SDS, and the ultraviolet (UV)/Visible (Vis) absorbance was measured in triplicate at 780 nm. ICG has a molar extinction coefficient of 2.621×10^5 $M^{-1}cm^{-1}$ at 780 nm (20). The ICG loading efficiency was therefore calculated using the following equation:

ICG loading efficiency (%) = concentration of ICG in purified nanoemulsion solution/concentration of ICG used for emulsion formulation ×100.

Size distribution and dispersion stability of ICG/PFCE nanoemulsions

The hydrodynamic size of ICG/PFCE nanoemulsions was analyzed using a zeta potential/particle sizer (Malvern Instrument, Malvern, UK). To check the dispersion stability of ICG/PFCE nanoemulsions, free ICG and ICG/PFCE nanoemulsions were dispersed in either PBS solution or DMEM cell culture medium (without phenol red) containing 10% FBS, respectively. The final concentration of ICG in the solutions was adjusted to 1 μM ICG equivalent. The solutions were maintained at 25 ℃ and the UV/Vis absorption spectra of the solutions analyzed for 48 h. In addition, hydrodynamic size and size distribution of the dispersed emulsions were measured for 14 days periodically.

^{19}F-MRI and Fluorescence imaging of ICG/PFCE nanoemulsions

Different concentrations of ICG/PFCE nanoemulsions dispersed in PBS were transferred into a 96-well plate. The final concentrations of ICG/PFCE nanoemulsion samples were 10, 20, 40, and 60 μM ICG equivalent, which corresponded to 15, 30, 60, and 90 mM fluorine equivalent, respectively. Fluorescence images were obtained using an IVIS Lumina (Caliper Life Sciences, Cy7 channel: excitation =710-760 nm, emission =810-875 nm).

^{19}F-MRI was performed using a 7 Telsa BioSpec (Bruker, Germany) MRI scanner. To obtain high resolution MR images, a home-made solenoid-type radiofrequency (RF) coil was constructed, which was tuned to [19]F

resonance frequency with 2 cm diameter and 4 cm length. ICG/PFCE nanoemulsions were imaged using a fast low angle shot (FLASH) MRI sequence with the following acquisition parameters: repetition time (TR)/echo time (TE) =100 ms/2.7 ms; 128×64 acquisition matrix; 20° flip angle; field of view (FOV) =2 cm.

Singlet oxygen generation of ICG/PFCE nanoemulsions during 810 nm laser irradiation

A singlet-oxygen-detecting reagent, singlet oxygen sensor green (SOSG) was dissolved in PBS (saturated with oxygen gas) containing either free ICG or ICG/PFCE nanoemulsions at 10 μM ICG equivalent. Each solution was irradiated with an 810 nm continuous wave (CW) laser at 2 W/cm². All experiments were performed in triplicate.

Measurement of temperature increase of free ICG and ICG/PFCE nanoemulsions during 810 nm laser irradiation

To check the photothermal effects, ICG/PFCE nanoemulsions and free ICGs were dispersed in PBS solution at various concentrations, and then irradiated with an 810 nm CW laser at 2 W/cm² for 5 min. During laser irradiation, the thermal image of each sample solution was recorded with an infrared camera (Thermovision A40, FLIR, Wilsonville, OR) in real time. Temperature changes were analyzed using the ThermaCAM Researcher software.

Cytotoxicity test

U87MG cells were seeded into 96-well plates at a density of 1×10^4 cells/well and incubated for 24 h for cell attachment. Free ICG and ICG/PFCE nanoemulsions were diluted with DMEM containing 10% FBS to obtain equivalent concentrations of 0, 10, 30, and 50 μM ICG. Cells were incubated in 200 μL of fresh medium containing free ICG or ICG/PFCE nanoemulsions for 4 h. For the untreated control group, cells were incubated in the same volume of fresh culture medium, without ICG for 4 h. Cells were then washed twice and further incubated in fresh culture medium for an additional 24 h. Cell viability of the treated and untreated control U87MG cells was measured using a cell counting kit-8 (CCK-8, Dojindo Laboratories, Japan). The absorbance was measured at 450 nm (reference =650 nm) using a microplate reader (Tecan Safire 2, Switzerland). Untreated control U87MG cells served as 100% viable
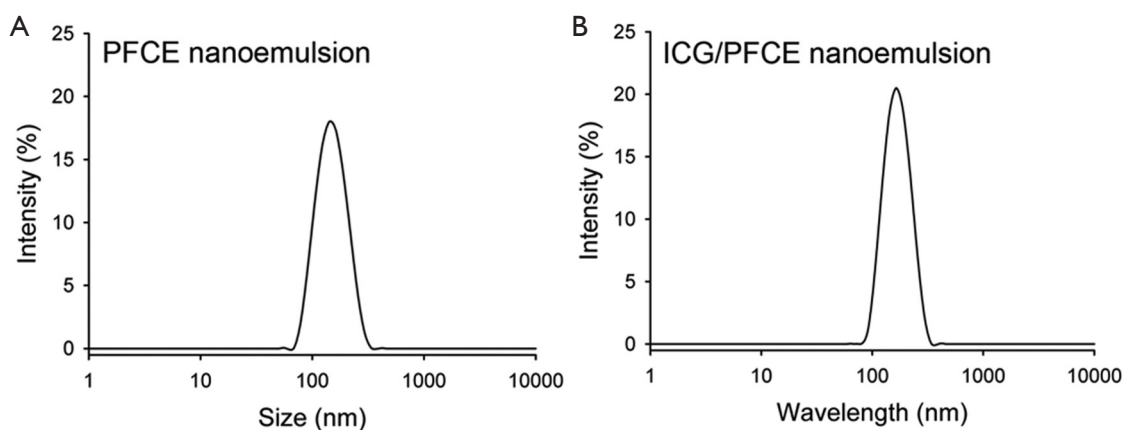
Figure 2 Hydrodynamic size distribution of (A) PFCE and (B) ICG/PFCE nanoemulsions in PBS solution

cells, and the medium served as the background. Data are expressed as mean ± SD from 4 data samples. Student's *t*-test was used for statistical analyses.

In vitro phototherapy of brain cancer

To check *in vitro* phototoxicity of the nanoemulsions, U87MG cells were seeded into a 96-well plate at a density of 1×10^4 cells/well and incubated for 24 h. Free ICG and ICG/PFCE nanoemulsions were diluted with DMEM containing 10% FBS to obtain equivalent concentrations of 0, 10, 30, and 50 μM ICG. The medium was replaced with 200 μL of fresh medium containing free ICG or ICG/PFCE nanoemulsions, followed by incubation for 4 h. The cells were washed twice and fresh cell culture medium was added. The cells were then irradiated with an 810 nm CW laser at 2 W/cm^2 for 5 min and incubated for an additional 24 h. Cell viability was measured using CCK-8. Data are expressed as the mean ± SD from 4 data samples.

To observe selective phototherapy of cancer by fluorescence microscopy, U87MG cells were seeded in 24-well plates at a density of 5×10^4 cells/well and incubated for 24 h for cell attachment. The existing culture medium was replaced with 500 μL of fresh medium containing free ICG or ICG/PFCE nanoemulsions (0, 10, 30, and 50 μM ICG equivalent), and incubated for 4 h. Cells were washed twice and fresh cell culture medium added. For PDT/PTT therapy, light was applied to the central part of the cell layer using an 810 nm CW laser (2 W/cm^2 for 5 min, light-spot diameter: 3.5 mm). Following illumination, the cells were immediately stained with calcein AM staining kit (Molecular Probes) for fluorescence microscopy of live and dead cells. Live cells were stained green with calcein (494/517 nm)

and the nuclei of dead cells were stained red with ethidium bromide dimer (528/617 nm). Fluorescent images were taken from >3 fields of view for each case. All the data were acquired using identical settings on the microscope in order to ensure reproducibility.

Results and discussion

Oil-in-water PFCE nanoemulsions were formulated using Lutrol® F68 as a surfactant, to reduce surface tension and produce a stable dispersion of nanoscale oil droplets in aqueous phase. Using laser dynamic light scattering, the hydrodynamic size of the nanoemulsion droplets without ICG was 160.4 nm (*Figure 2A*) and this was not affected by ICG loading (164.2 nm) (*Figure 2B*).

ICG was efficiently encapsulated in the nanoemulsion droplets, with an encapsulation efficiency of 74%, as analyzed by UV/Vis absorption. The stability of ICG/PFCE nanoemulsions in aqueous solution was also investigated by UV/Vis spectrophotometry (*Figure 3*). The absorbance of free ICG in PBS solution was shown to rapidly decrease by 53% after 24 h and by 83% after 48 h, respectively. This decrease in UV/Vis absorbance may be due to the aqueous instability of ICG and subsequent physicochemical transformation as reported previously (13). In contrast, ICG loaded in nanoemulsion formulation showed much smaller changes in UV/Vis absorbance with only a 21% decrease in UV/Vis absorbance after 48 h incubation. These results indicate that the stability of ICG was significantly improved when ICG was loaded in nanoemulsion formulation. The dispersion stability of ICG/PFCE nanoemulsions in DMEM containing 10% FBS was also investigated to determine whether serum proteins may
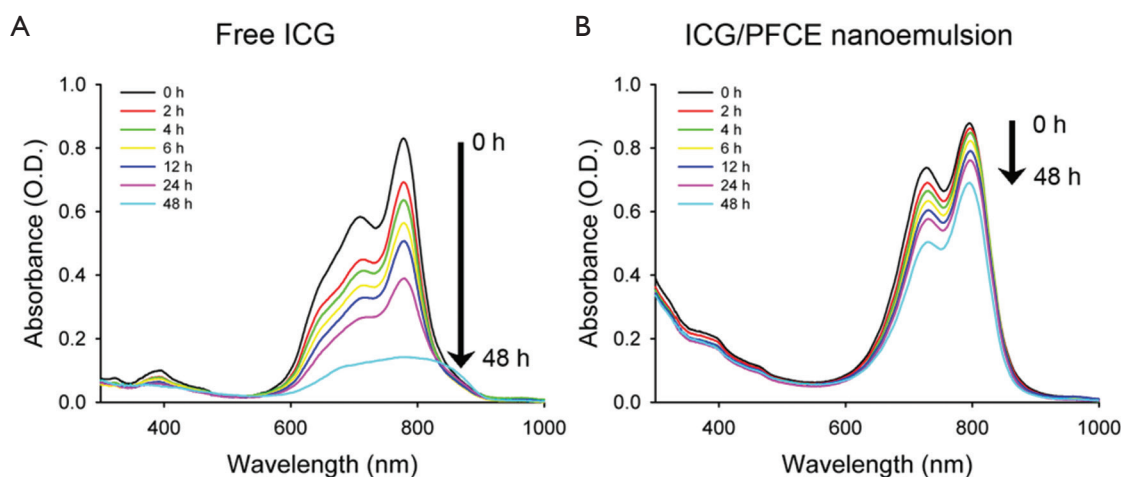
136

Wang et al. ICG/PFCE nanoemulsions for bimodal ^{19}F-MR/NIRF

Figure 3 Changes in the UV/Vis spectra of (A) free ICG and (B) ICG/PFCE nanoemulsions with time. Both agents were dissolved in PBS solution, and their UV/Vis absorbance was measured periodically for 48 h
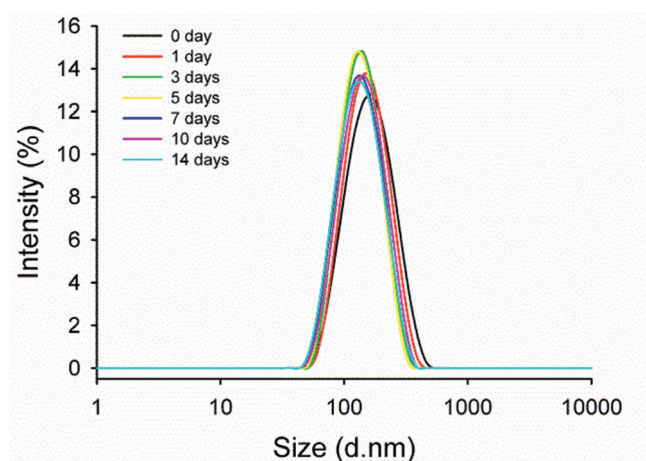

Figure 4 Changes in hydrodynamic size distribution of ICG/PFCE nanoemulsions with time. The nanoemulsion was dispersed in DMEM containing 10% FBS, and its size distribution was analyzed for 14 days

destabilize the nanoemulsion by adsorbing on the emulsion surface. During a 2-week incubation in serum-contained media, no significant change in ICG/PFCE size distribution was observed (*Figure 4*). These results demonstrate that the surfactant F68 effectively prevents serum proteins from accessing the emulsion surface.

The utility of ICG/PFCE nanoemulsions as a bimodal imaging agent for ^{19}F-MRI and NIRF was evaluated using different concentrations of nanoemulsion solutions. The signal intensity of ^{19}F-MRI was shown to be enhanced with increasing concentration of ICG/PFCE (*Figure 5A*)

while no signal came from the surrounding background. These results suggest that delivery of this nanoemulsion to tumors may be traced and visualized with a high signal-to-background ratio using ^{19}F-MRI, and its concentration at the target site may be analyzed quantitatively.

NIRF is a highly sensitive imaging modality compared with other imaging modalities even though the depth of tissue penetration is limited to <10 cm (21). We examined the NIRF images of ICG/PFCE nanoemulsions at 10-μM ICG equivalent to the ^{19}F-MRI signal intensity images at this concentration was relatively weak. *Figure 5B* shows that PFCE nanoemulsions without ICG did not generate NIRF while clear and highly bright fluorescence images were obtained with ICG/PFCE nanoemulsions (10 μM ICG equivalent). These data suggest that bimodal ^{19}F-MR and NIRF imaging using ICG/PFCE nanoemulsions may enable *in vivo* tracing and visualization of the nanoemulsion with high signal-to-background ratio and no depth limitation. In addition, real-time and highly sensitive fluorescence imaging could be performed to determine tumor sites during surgery or for subsequent phototherapy.

Next, we compared ability of free ICG and ICG/PFCE nanoemulsion to generate singlet oxygen at a concentration of 10-μM ICG equivalent (*Figure 6*). Singlet oxygen ($^1O_2$) is the most important reactive oxygen species for PDT. When photosensitizers are excited with an appropriate light, it transfers its energy to surrounding molecular oxygen thereby generating highly reactive $^1O_2$, which can cause cell damage, ultimately leading to cell death. As shown in *Figure 6*, fluorescence of singlet oxygen sensor
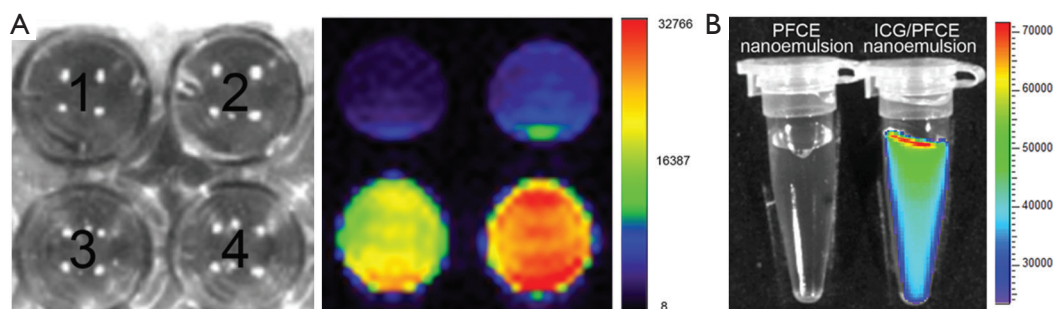
Figure 5 ^{19}F-MR and NIRF images of ICG/PFCE nanoemulsion solutions. A. bright field images of 96 well plate containing ICG/PFCE nanoemulsions with different concentrations of fluorine (left picture): [1] 15 mM ^{19}F (corresponding to 10 µM ICG), [2] 30 mM ^{19}F (20 µM ICG), [3] 60 mM ^{19}F (40 µM ICG) and [4] 90 mM ^{19}F (60 µM ICG), respectively. Right picture is the corresponding 19F-MR image; B. NIRF images of microtubes containing PFCE and ICG/PFCE nanoemulsions. The emulsion concentration corresponded to 10 µM ICG equivalent
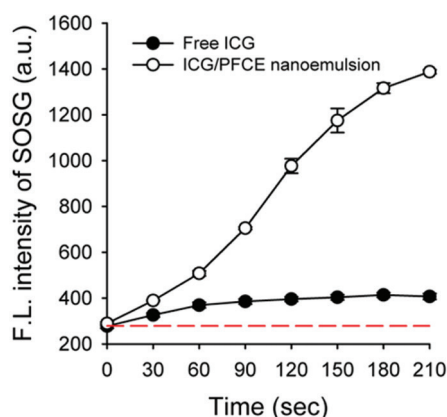

Figure 6 Time-dependent singlet oxygen generation of free ICG and ICG/PFCE nanoemulsion during light irradiation (810 nm CW laser, light dose rate: 2 W/cm^2). The dashed line represents baseline SOSG fluorescence

green (SOSG) gradually increased with time during light illumination, indicating continuous generation of singlet oxygen by ICG. Interestingly, singlet oxygen generation (SOG) of ICG/PFCE nanoemulsions was 8.3 times greater than that of free ICG. This may be due to a difference in oxygen concentration between free ICG and ICG/PFCE nanoemulsion. PFCs are known to have high oxygen-dissolving capacities (~40-50 vol%), as compared with 2.5 vol% for water (19). Therefore, even though aqueous solutions may be saturated with oxygen before light irradiation, the ICG/PFCE nanoemulsions may have much greater amount of oxygen compared with free ICG-dispersed aqueous solution.

Figure 7 shows the photothermal effects of ICG/PFCE nanoemulsions. Free ICG and ICG/PFCE

nanoemulsions effectively generated heat upon NIR laser irradiation whereas PFCE nanoemulsion alone had no ability to generate photothermally-induced heat in these conditions (see thermographic image in *Figure* 7*B*). The temperature of the sample solutions rapidly rose within 2 min of laser irradiation and gradually lowered again thereafter. According to Saxena *et al.* (13), ICG degradation in aqueous media can be accelerated by light exposure or at high temperature. Therefore, the decrease in solution temperature after reaching peak temperature appears to be due to irreversible degradation of ICG dye, and subsequent loss of its ability for light absorption and heat generation. The temperature increase was found to be slightly higher for free ICG solution than for ICG/PFCE nanoemulsion.

Previous studies have shown that the condition for thermal therapy of cancer is dependent on the operating temperature (22,23). For example, 1 h is required to induce irreversible cellular damage at 46 ℃, while only 4-6 min is sufficient at 50-52 ℃. At temperatures greater than 60 ℃, rapid cellular damage occurs because of the almost instantaneous induction of protein coagulation. Therefore, from the data in *Figure* 7, the photo-induced thermal effects become more important at increased concentrations of ICG/PFCE nanoemulsions, and therefore both photodynamic and photothermal effects at higher ICG concentrations can induce cancer cell death. At treatment conditions below 30 µM ICG equivalent, therapeutic outcome will depend on singlet oxygen generation.

Cytotoxicity of free ICG and ICG/PFCE nanoemulsions was examined by incubation of U87MG cancer cells with these agents, followed by measurement of cell viability without light irradiation. Both free ICG and the nanoemulsions were found to be highly biocompatible
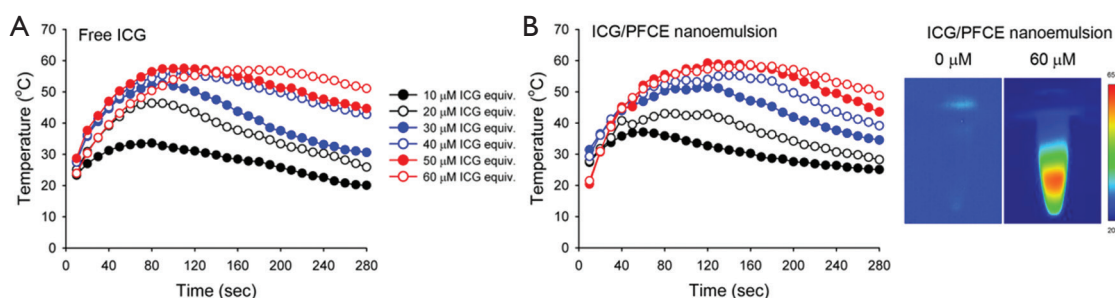
138

Wang et al. ICG/PFCE nanoemulsions for bimodal ^{19}F-MR/NIRF

Figure 7 Temperature variation of (A) free ICG and (B) ICG/PFCE nanoemulsions during light illumination with an 810 nm CW laser (light dose rate: 2 W/cm^2). Representative thermographic images of PFCE (0 µM ICG equivalent) and ICG/PFCE nanoemulsions (60 µM ICG equivalent) are shown on the right side
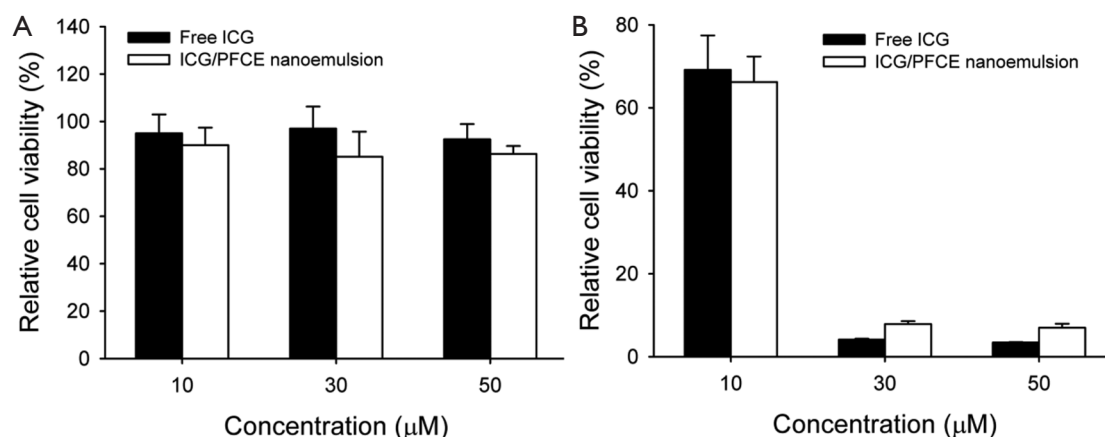

Figure 8 A. Cell viability of U87MG cells treated with free ICG and ICG/PFCE nanoemulsion at various concentrations of ICG equivalent; B. *In vitro* phototoxicity of U87MG cells treated with free ICG or ICG/PFCE nanoemulsion for 4 h at 0, 10, 30, and 50 µM ICG equivalent, and then irradiated with an 810 nm CW laser (2 W/cm^2 for 5 min). Data expressed as the mean ± S.D. (n=4)

although minor cell death was observed in the cells treated with ICG/PFCE nanoemulsions (*Figure 8A*). Phototoxicity of free ICG and ICG/PFCE treated cells was also evaluated (*Figure 8B*). When U87MG cells treated with free ICG were irradiated with NIR light, cell viability fell to 69%, 4.3%, and 3.6% for cells treated with 10, 30, and 50 µM ICG, respectively. When U87MG cells treated with ICG/ PFCE nanoemulsions were irradiated with NIR light, cell viability was 66%, 7.8%, and 6.9% for the cells treated with 10, 30, and 50 µM ICG equivalent, respectively. These results indicated that both free ICG and the nanoemulsions were effective in killing glioblastoma cells *via* photo-induced singlet oxygen generation and hyperthermia. Despite similar phototoxic effects for free ICG and the nanoemulsions, we speculate that ICG/PFCE nanoemulsions may induce a much better therapeutic outcome *in vivo* rather than free ICG. Free ICG has a short blood half-life (2-4 min), and

therefore it is difficult to obtain sufficient tumor uptake for therapy *in vivo*. In contrast, nano-sized emulsion formulation showing good stability in serum-containing aqueous solution (*Figures 3,4*) would have a prolonged blood circulation time which is important for passive targeting of cancers *via* enhanced permeability and retention (EPR) effect (24).

The PDT/PTT effect of ICG/PFCE nanoemulsions was further evaluated using fluorescence microscopy. U87MG cells treated with free ICG and ICG/PFCE nanoemulsions were irradiated with an 810 nm CW laser for 5 min, and stained with calcein AM for fluorescence microscopy (*Figure 9*). Cells treated with 30 and 50 µM ICG equivalent and irradiated with a NIR laser were mostly stained red in the light-illuminated region, indicating that light illumination induced immediate necrotic cell death at these high ICG concentrations. As expected, cells treated
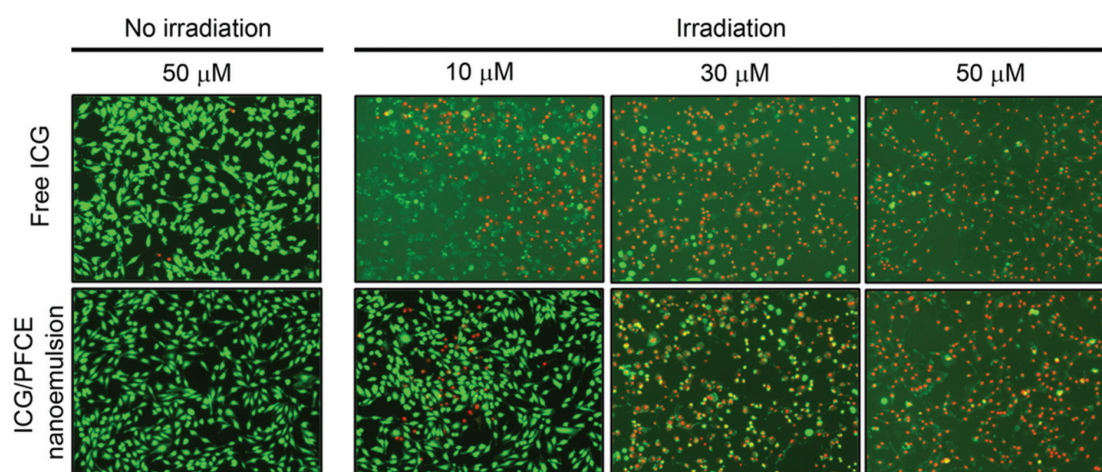
Figure 9 U87MG glioblastoma cells treated with free ICG and ICG/PFCE nanoemulsion at different concentrations were stained using Calcein AM following irradiation using an 810 nm CW laser. Live cells are shown in green while dead cells appear in red. U87MG cells treated with 50 µM free ICG or ICG/PFCE nanoemulsion was also stained without laser irradiation

with 10-µM ICG equivalent and irradiated with NIR light underwent less cell death. Cells treated with free ICG and ICG/PFCE nanoemulsions at 50 µM equivalent without light irradiation were shown to have healthy morphologies and mostly stained with green fluorescence. This confirms that ICG/PFCE nanoemulsion is highly biocompatible and nontoxic to cells at this high concentration.

Conclusions

We conclude that ICG/PFCE nanoemulsion is useful not only as a ^{19}F-MR and NIRF bimodal imaging agent but is also helpful for improving the aqueous stability of ICG. Cytotoxicity tests and fluorescence microscopy studies confirmed that this nanoemulsion is highly biocompatible with only minor toxicity. Upon light irradiation, U87MG glioblastoma cells incubated with the nanoemulsions underwent necrotic cell death. The therapeutic mechanism during light illumination appears to be mainly due to the photodynamic effect at lower concentrations of ICG while the photothermal effect became more obvious at increased ICG concentration, enabling combined photodynamic/photothermal therapy of cancer cells.

Acknowledgements

References

1. Choi KY, Liu G, Lee S, et al. Theranostic nanoplatforms for simultaneous cancer imaging and therapy: current approaches and future perspectives. Nanoscale 2012;4:330-42.
2. Caldorera-Moore ME, Liechty WB, Peppas NA. Responsive theranostic systems: integration of diagnostic imaging agents and responsive controlled release drug delivery carriers. Acc Chem Res 2011;44:1061-70.
3. Wang P, Moore A. Theranostic magnetic resonance imaging of type 1 diabetes and pancreatic islet transplantation. Quant Imaging Med Surg 2012;2:151-62.
4. Riess JG. Oxygen carriers ("blood substitutes")--raison d'etre, chemistry, and some physiology. Chem Rev 2001;101:2797-920.
5. Srinivas M, Heerschap A, Ahrens ET, et al. ^{19}F MRI for quantitative in vivo cell tracking. Trends Biotechnol 2010;28:363-70.
6. Janjic JM, Ahrens ET. Fluorine-containing nanoemulsions for MRI cell tracking. Wiley Interdiscip Rev Nanomed Nanobiotechnol 2009;1:492-501.
7. Gibbs SL. Near infrared fluorescence for image-guided surgery. Quant Imaging Med Surg 2012;2:177-87.

8. Lee JH, Park G, Hong GH, et al. Design considerations for targeted optical contrast agents. Quant Imaging Med Surg 2012;2:266-73.

9. Schaafsma BE, Mieog JS, Hutteman M, et al. The clinical use of indocyanine green as a near-infrared fluorescent contrast agent for image-guided oncologic surgery. J Surg Oncol 2011;104:323-32.

10. Polom K, Murawa D, Rho YS, et al. Current trends and emerging future of indocyanine green usage in surgery and oncology: a literature review. Cancer 2011;117:4812-22.

11. Yanina IY, Tuchin VV, Navolokin NA, et al. Fat tissue histological study at indocyanine green-mediated photothermal/photodynamic treatment of the skin in vivo. J Biomed Opt 2012;17:058002.

12. Kuo WS, Chang YT, Cho KC, et al. Gold nanomaterials conjugated with indocyanine green for dual-modality photodynamic and photothermal therapy. Biomaterials 2012;33:3270-8.

13. Saxena V, Sadoqi M, Shao J. Degradation kinetics of indocyanine green in aqueous solution. J Pharm Sci 2003;92:2090-7.

14. Saxena V, Sadoqi M, Shao J. Enhanced photo-stability, thermal-stability and aqueous-stability of indocyanine green in polymeric nanoparticulate systems. J Photochem Photobiol B 2004;74:29-38.

15. Desmettre T, Devoisselle JM, Mordon S. Fluorescence properties and metabolic features of indocyanine green (ICG) as related to angiography. Surv Ophthalmol 2000;45:15-27.

16. Kirchherr AK, Briel A, Mäder K. Stabilization of indocyanine green by encapsulation within micellar systems. Mol Pharm 2009;6:480-91.

17. Li J, Jiang H, Yu Z, et al. Multifunctional uniform core-shell Fe3O4@mSiO2 mesoporous nanoparticles for bimodal imaging and photothermal therapy. Chem Asian J 2013;8:385-91.

18. Sharma P, Bengtsson NE, Walter GA, et al. Gadolinium-doped silica nanoparticles encapsulating indocyanine green for near infrared and magnetic resonance imaging. Small 2012;8:2856-68.

19. Lowe KC. Engineering blood: synthetic substitutes from fluorinated compounds. Tissue Eng 2003;9:389-99.

20. Yuan B, Chen N, Zhu Q. Emission and absorption properties of indocyanine green in Intralipid solution. J Biomed Opt 2004;9:497-503.

21. Rudin M, Weissleder R. Molecular imaging in drug discovery and development. Nat Rev Drug Discov 2003;2:123-31.

22. Goldberg SN, Gazelle GS, Halpern EF, et al. Radiofrequency tissue ablation: importance of local temperature along the electrode tip exposure in determining lesion shape and size. Acad Radiol 1996;3:212-8.

23. Thomsen S. Pathologic analysis of photothermal and photomechanical effects of laser-tissue interactions. Photochem Photobiol 1991;53:825-35.

24. Hashizume H, Baluk P, Morikawa S, et al. Openings between defective endothelial cells explain tumor vessel leakiness. Am J Pathol 2000;156:1363-80.